

2001

Observations of Intratidal Variability of Flows Over a Sill/Contraction Combination in a Chilean Fjord

Arnoldo Valle-Levinson
Old Dominion University

Fernando Jara

Carlos Molinet

Doris Soto

Follow this and additional works at: https://digitalcommons.odu.edu/ccpo_pubs

 Part of the [Oceanography Commons](#)

Repository Citation

Valle-Levinson, Arnoldo; Jara, Fernando; Molinet, Carlos; and Soto, Doris, "Observations of Intratidal Variability of Flows Over a Sill/Contraction Combination in a Chilean Fjord" (2001). *CCPO Publications*. 269.
https://digitalcommons.odu.edu/ccpo_pubs/269

Original Publication Citation

Valle-Levinson, A., Jara, F., Molinet, C., & Soto, D. (2001). Observations of intratidal variability of flows over a sill/contraction combination in a Chilean fjord. *Journal of Geophysical Research: Oceans*, 106(C4), 7051-7064. doi:10.1029/2000jc900157

Observations of intratidal variability of flows over a sill/contraction combination in a Chilean fjord

Arnoldo Valle-Levinson,¹ Fernando Jara,² Carlos Molinet,³ and Doris Soto⁴

Abstract. Underway velocity measurements were carried out for the first time in a Chilean fjord using an acoustic Doppler velocimeter with the purpose of elucidating the intratidal variability of flows through a pass, Paso Galvarino. The pass included a sill, where the bottom sloped by roughly 30%, and a coastline contraction of ~90%. The relatively small dimensions of the pass allowed for rapid sampling of the flow evolution throughout the tidal cycle. The backscattered sound signal from the velocimeter and from an echo sounder were used to describe the vertical excursions of the pycnocline throughout the domain and to identify regions of enhanced vertical mixing within the pass. The spatial variability of the flow in the pass was consistent with uniform two-layer flow. At the narrowest section of the contraction the pycnocline dropped sharply around both maximum flood and maximum ebb, while the flow accelerated downstream relative to the tidal flow. The slope of the pycnocline changed sign from flood to ebb, which was atypical of other fjord observations but could be explained by the transitions from subcritical to supercritical flow. These transitions switched location at either side of the narrowest section of the contraction. Leeward of this section, increased sound backscatter suggested intensified turbulence that extended over a greater area during ebb than during flood because the distance between the point of pycnocline drop and the end of the pass was longer during ebb. Enhanced vertical mixing within the pass was reflected in the tidally averaged fields by a three-layer flow that consisted of near-surface and near-bottom flow converging toward the pass and flow around the pycnocline diverging away from the pass.

1. Introduction

Oceanic flows over sills and through coastline contractions determine the water characteristics at either side of the morphological constriction and have been the focus of numerous investigations. These studies have established a hydraulic exchange two-layer theory that has been described by *Farmer and Freeland* [1983]. Many of the studies on hydraulic exchange have been summarized by *McClimans* [1990] and by *Bryden and Kinder* [1991]. Solutions to exchange over a sill have been proposed for steady two-layer [e.g., *Stommel and Farmer*, 1952, 1953; *Armi*, 1986] and three-layer [*Pratt et al.*, 1999] scenarios unaffected by barotropic flow, steady cases influenced by rotation [e.g., *Gill*, 1977; *Bormans and Garrett*, 1989; *Borenäs and Pratt*, 1990; *Dalziel*, 1990; *Pratt and Lundberg*, 1991; *Killworth*, 1992; *Killworth and McDonald*, 1993], scenarios modified by barotropic flow without rotation [e.g., *Stigebrandt*, 1977;

Armi and Farmer, 1986; *Farmer and Armi*, 1986], cases forced by one cycle of prescribed oscillatory barotropic flow [e.g., *Geyer*, 1990; *Matsuura and Hibiya*, 1990; *Helfrich*, 1995], and scenarios affected by the fortnightly modulation of tidal forcing [e.g., *Hibiya and LeBlond*, 1993; *Hibiya et al.*, 1998].

The inclusion of frictional effects in some of the above studies and in additional investigations has shown that the internal hydraulic control obtained by frictionless solutions may be drastically modified or broken by mixing [e.g., *Gan and Ingram*, 1992; *Johnson and Ohlsen*, 1994; *Valle-Levinson and Wilson*, 1994a, 1998; *Hibiya et al.*, 1998]. In particular, the pycnocline instabilities and the vertical mixing produced by the interaction of tidal flow with stratified fluid over a sill and/or contraction have been observed to affect the long-term exchange of volume and material between two basins [e.g., *Geyer and Cannon*, 1982; *Stacey*, 1984; *Griffin and LeBlond*, 1990; *Valle-Levinson and Wilson*, 1994b; *Cudaback and Jay*, 1996]. Several investigations on the transient interaction between tidal flow and bottom topography in stratified systems have focused on the generation of internal waves and instabilities and have concentrated only on one portion of the tidal cycle [e.g., *Hauray et al.*, 1979; *Farmer and Smith*, 1980; *Farmer and Denton*, 1985; *Farmer and Armi*, 1999; *Klymak and Gregg*, 1998].

Despite a substantial body of literature on theoretical hydraulic exchange and notwithstanding the fact that natural systems experiencing hydraulic exchange flows are usually influenced by strong tidal forcing (e.g., Gibraltar Strait, North American fjords, South American fjords, and Scandinavian fjords) there are only few reported observations on the variability of the exchange flows throughout one com-

¹Center for Coastal Physical Oceanography, Department of Ocean, Earth, and Atmospheric Sciences, Old Dominion University, Norfolk, Virginia.

²Laboratorio de Ecología Acuática, Puerto Montt, Chile.

³Centro Universitario de La Trapananda, Universidad Austral de Chile, Coyhaique, Chile.

⁴Facultad de Pesquerías y Oceanografía, Universidad Austral de Chile, Puerto Montt, Chile.

plete tidal cycle [Farmer and Armi, 1988; Marsden and Greenwood, 1994]. Those studies have been carried out in systems with large dimensions that complicate the synoptic sampling and portrayal of exchange flows at different phases of the tidal cycle. This study, although preliminary in nature, was motivated by the shortage of information on tidal variability of flows over sills and contractions and might serve to stimulate additional investigations of this kind. Its objectives are 1) to describe the intratidal variability of flows over a combination of sill/contraction in a natural system, and 2) to assess the observed variability in the context of existing theories. The objectives are pursued with observations of a towed acoustic Doppler current profiler (ADCP) and of conductivity-temperature-depth (CTD) profiles at either side of a sill/contraction combination in a Chilean fjord throughout one semidiurnal tidal cycle. This is the first time that an ADCP has been used to measure currents in a Chilean fjord. The study area is described next, followed by the data collection and processing techniques. Then, a description of the temporal variability of density profiles at either side of the contraction and a comparison of density and sound backscatter profiles is presented to justify the use of backscatter profiles as proxy for pycnocline variability in space and time. This is followed by a description of the flow and pycnocline variability, corroborated by echo sounder measurements. Assessment of observations in the context of theory is carried out by placing our observations in the context of the Froude number of the undisturbed flow F_0 and of the ratio between the height of the sill and the lower layer thickness [Baines, 1995]. In addition, the observations are put into the context of upper and lower layer Froude numbers and also associated to the work of Hibiya *et al.* [1998]. This manuscript concludes with a summary of the main findings.

2. Study Area

The sill/contraction combination where this study concentrates is known as Paso Galvarino, a pass connecting the northern and southern portions of Seno Ventisquero, a fjord in southern Chile (Figure 1). Seno Ventisquero is oriented at nearly 11° true and at its southernmost end is connected to Canal Jacaf and Canal Puyuguapi, both of which lead to the Chilean Inland Sea. The Paso Galvarino, also referred to as "the pass," represents a 90% coastline constriction along 1500 m of the fjord. At the pass, the width of the fjord decreases from roughly 2000 m to nearly 200 m. The northern side of the pass is landward or toward the head of the fjord, and the southern side of the pass is toward the mouth of the fjord. The depth changes from 40 m on the landward side of the pass to 8 m at the shallowest portion of the sill and to 80 m south of the pass. The area of the basin to the north of the pass Y is $\sim 10^7$ m² and that of the narrowest cross section of the pass A is ~ 2000 m² (200×10 m).

The fjords in southern Chile, in general, are characterized by well-defined pycnoclines [Pickard, 1971] and large tidal amplitudes. In the region of Canal Puyuguapi and Seno Ventisquero, there is a number of nongauged freshwater streams and rivers that discharge on either side of Paso Galvarino. The pycnocline is usually shallower than 10 m and has typical vertical gradients of 2-3 σ_t /m. This pycnocline remains well defined throughout the fjords despite the forcing by tides, and the horizontal density gradients remain relatively weak [Silva *et al.*, 1995]. Although direct velocity measurements in the area of the Chilean Inland Sea are very

scarce, the tidal amplitude at the northern entrance to the Chilean Inland Sea, around Chacao channel, is typically 4 m. In contrast, in Paso Galvarino, variations of sea level observed on the shorelines during our sampling period suggested a semidiurnal tidal amplitude a of ~ 1 m. The properties of the pass should then yield an amplitude of the tidal current u_0 that equals $aY\sigma/A$ [Stigebrandt, 1977] or 0.5 m/s, where σ is the frequency of the semidiurnal tide ($2\pi/12.42$ h). As seen at Paso Galvarino, the tidal currents are of the order of 0.5 m/s, consistent with its geometry, and are energetic enough to interact with the bathymetry to modify the position of the pycnocline in the water column and to enhance vertical mixing within the pass.

Owing to the relatively small dimensions of Paso Galvarino, its length can be sampled quasi-synoptically (15-20 min). This advantageous sampling situation, combined with the well-established density stratification and tidal forcing conditions, make the pass an ideal natural laboratory to study the effects of oscillatory barotropic forcing on flows over sills and contractions.

3. Data Collection

Velocity profiles through the pass were combined with density profiles at either side of the pass and with high-resolution echo sounding records during spring tides of one semidiurnal cycle on January 12, 1998. In addition, across fjord transects were sampled on either side of the pass (Figure 1). The purpose of the sampling strategy was to resolve the intratidal variability of the flows through the contraction/sill combination and to elucidate the transverse structure of the flows entering and leaving the pass. A total of eight sampling cycles of the trajectory of Figure 1 (white dots) were accomplished during the 12 hours of measurements. The along-pass transect was surveyed 15 times as it was traversed in both directions during the sampling circuit. In this work, we concentrate only on the flows within the pass, i.e., on the along-fjord transect that was sampled 15 times and on the CTD stations sampled at either side of the pass. The flow at both sides of the pass exhibited substantial transverse shears and recirculations due to the presence of the constriction.

Velocity profiles were obtained with a broadband 600 kHz RD Instruments ADCP. The ADCP was towed on a 1.2 m-long catamaran along the starboard side of the R/V *Arturo Pratt* (of the Technical Fisheries Institute in Puerto Cisnes, Chile) at speeds between 2 and 2.5 m/s. Each transect along Paso Galvarino took between 15 and 20 min. Velocity profiles with a vertical resolution (bin size) of 0.5 m and ping rates of ~ 1 Hz were averaged every 15 s, yielding a spatial resolution of ~ 30 -40 m. The ADCP compass was calibrated as given by Trump and Marmorino [1997] using Global Positioning System (GPS) navigation data. Sound backscatter, as recorded by the ADCP, was used to describe variations of the pycnocline position along the pass and to identify regions of enhanced turbulence. This is justified in section 4 by comparing density and backscatter profiles and is also validated by echo sounder records.

Density profiles were measured with a Hydrolab Data-sonde 4 CTD multiprobe. The accuracy of the salinity and temperature measurements was ± 0.2 and $\pm 0.1^\circ\text{C}$, respectively, and the resolution of these measurements was 0.01 for salinity and 0.01°C for temperature. Problems with the pressure sensor during the CTD casts invalidated the values below depths of ~ 14 m. Density values were obtained from measured temperature, salinity, and pressure with the

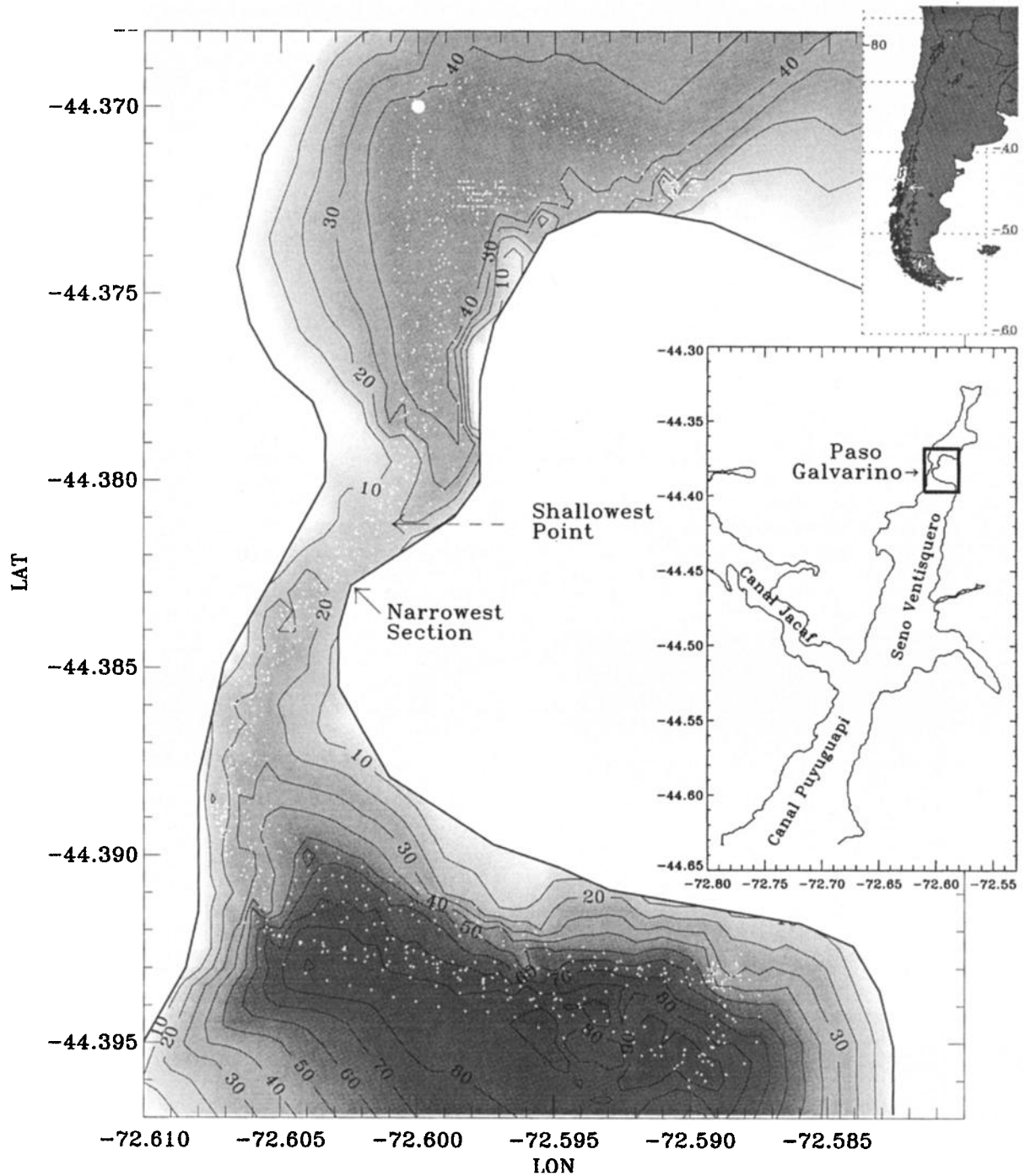


Figure 1. Area of study featuring Paso Galvarino. The upper right insert shows the region of South America (white arrow) where the study took place. The middle right insert represents a detailed view of the fjords and inlets around Paso Galvarino. The bathymetry of Paso Galvarino is contoured every 10 m, from 0 to 90 m with solid contours. Shaded contours are presented at 10 m intervals from 5 to 95 m. The shallowest point of the sill and the narrowest section are pointed out. The location where the along-fjord sections (Figures 4 to 8) begin is denoted by a white filled circle at -44.37°N , -72.60°W . White dots represent the location of ADCP flow and backscatter measurements.

international equation of state of seawater [e.g., Gill, 1982]. The sampling rate of the CTD was 0.2 Hz, thus making each CTD cast a time-consuming task (~ 10 min). The long time consumed on each CTD cast hindered density measurements inside the pass because the ship drift caused by stopping would have lessened the ADCP data quality and spatial resolution.

In addition to ADCP and CTD data, underway echo soundings were recorded on paper with a 50 kHz Furuno FE-6300 echo sounder. Not only did the echo sounder trace provided a high-spatial resolution bathymetry, it also was an effective representation of the pycnocline position in the water column. This validated the interpretation of the ADCP backscatter data, which were of relatively lower spatial

resolution. Echo sounder records were available for 12 out of 15 traverses of the pass. The paper records were scanned to produce digital images that were then cropped to the area of the pass. The image obtained by every other crossing was rotated 180° around the ordinate to consistently portray the same orientation for every traverse.

4. Data Description

In order to study the dynamics of flows in a pass, it is necessary to discern the distribution of the density (ρ) and the flow fields at either side and within the pass. Of particular relevance is the determination of the pycnocline position in the water column and how it changes as a consequence of morphologic influences. In the present work, the flow field is resolved adequately with ADCP measurements. However, the density field is only known at both sides of the pass. Therefore it is necessary for the purpose of this study to use a proxy of the density field and/or the pycnocline. Time series of water density and sound backscatter profiles (from the 600 kHz ADCP) at both sides of the pass showed similar variability (Figure 2). The upper, fresher layer featured continuously stratified density values in the range 1010-1015 kg/m^3 . This upper layer was ~5 m

thick on the northern (toward the head of the fjord) side of the pass and was only weakly perturbed by tidal forcing. On the southern (toward the mouth) side of the pass, the upper layer thickness changed more than to the north, roughly traced by the 15 σ_t isopycnal in the time series and by the maximum backscatter (b) at each time in the time series.

Analogous variability was identified from the time series profiles of the squared buoyancy frequency ($g/\rho \Delta\rho/\Delta z$, where g is the acceleration owing to gravity and z is the vertical coordinate) and of the vertical gradient of ADCP backscatter ($\Delta b/\Delta z$) (Figure 3), calculated from the time series shown in Figure 2. The vertical excursions of the pycnocline were greater to the south (Figures 3b and 3d) of the pass than to the north (Figures 3a and 3c). This was most probably due to ebb instabilities and fresh water being mixed downward, similarly to observations in Observatory Inlet, British Columbia [Farmer and Denton, 1985]. As shown later, the horizontal extent of vertical mixing was greater during ebb than during flood because the distance between the point of mixing initiation and the end of the pass was longer during ebb. During flood, the instabilities likely remained seaward of the CTD station located to the north. The instabilities of the pycnocline and related hydraulic effects were illustrated by the sections along the

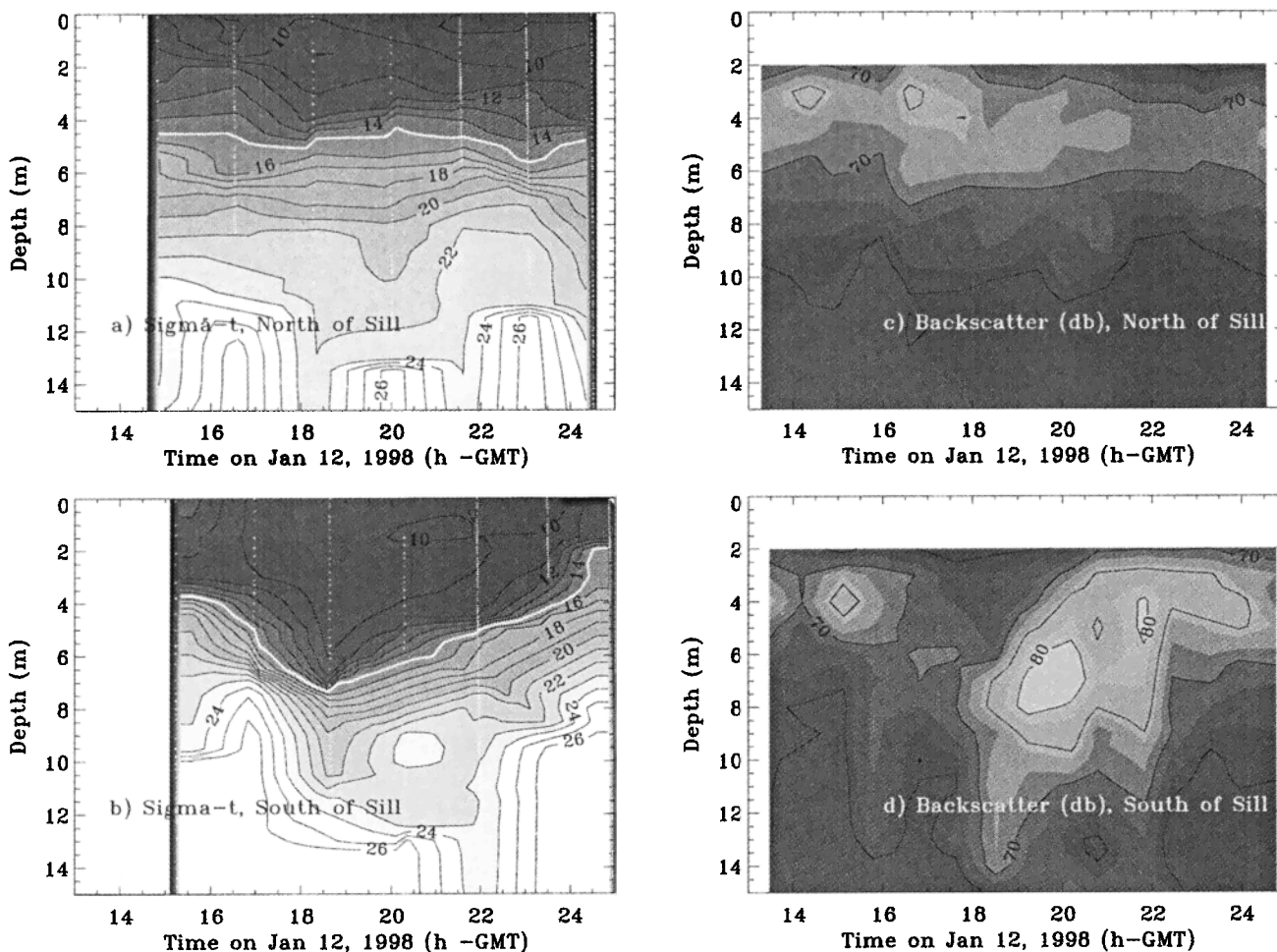


Figure 2. Time series of density (σ_t , in kg/m^3) and backscatter (decibels) profiles at either side of the strait. The white dots on the σ_t plots denote the time and depth when the measurements took place. The white contour represents the 15 σ_t isopycnal, emulating the approximate central portion of the pycnocline. Contour interval is 1 kg/m^3 . The backscatter plots feature contours at intervals of 5 decibels.

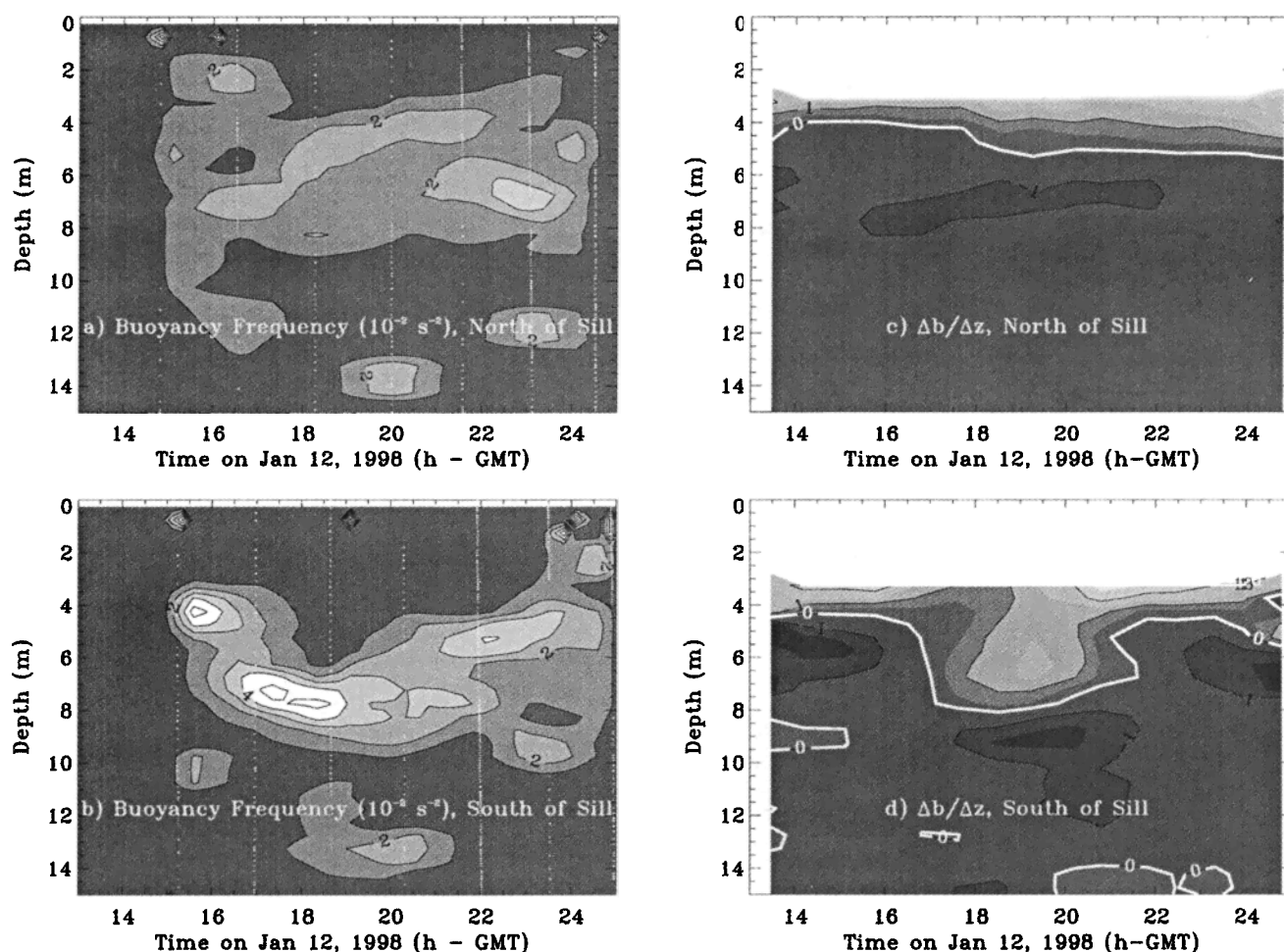


Figure 3. Time series of buoyancy frequency (s^{-2}) and vertical gradient of backscatter. High values of buoyancy frequency in Figures 3a and 3b denote the location of the pycnocline. Contour interval is $0.01 s^{-2}$. In Figure 3c and 3d, zero vertical gradients (or maxima) of backscatter (white contour) represent the approximate position of the pycnocline.

pass of echo sounder trace, flow, and backscatter (Figs. 4 through 8). The importance of Figures 2 and 3 resides in the fact that they provided confidence for the use of the backscatter signal as a proxy for the position of the pycnocline. Maximum ADCP backscatter nearly coincided with maximum density stratification. This is not surprising as the sound backscatter, as recorded by echo sounders, has been used in numerous studies to describe the spatial variability of the pycnocline induced by tidal flows interacting with bathymetry in strongly stratified systems [e.g., Farmer and Smith, 1980; Farmer and Denton, 1985; Farmer and Armi, 1999; Klymak and Gregg, 1998]. The density field, however, was not correlated to the backscatter signal, and unfortunately there was no information on the distribution of the water density inside the pass. Thus the variability of the flow and pycnocline position induced by the interaction of barotropic forcing with morphologic influences is explored next throughout one tidal cycle.

At the beginning of the experiment the pycnocline was well outlined as it bulged up just to the south (upstream) of the narrowest point of the pass (Figure 4a). This pycnocline bulging was in agreement with the numerical results of Valle-Levinson and Wilson [1994a] and of Helfrich [1995]. At the point between 1.3 and 1.4 km (e.g., Figure 4b), the

pycnocline then dropped rapidly and became diffuse owing to the internal motions excited by the morphology of the pass. To the north of the pass the pycnocline was again well defined and appeared near the depth where it was to the south of the pass. The position of the pycnocline was also well represented by the maximum ADCP backscatter (Figure 4b). The echo sounder recording interval was smaller than that of the ADCP backscatter and therefore had higher spatial resolution and better delineated the bathymetry and the pycnocline oscillations associated with the sill/contraction combination.

The flow measurements (Figure 4b) indicated that the experiment began ~ 1 hour before maximum flood, i.e., flow toward the north. Tidal forcing was strong enough within the pass to produce unidirectional (almost depth-independent) flow. The unidirectional flood flow decelerated at the northern end of the pass as the depth increased and the coastline widened. Associated with this deceleration, the generation of transverse flows and recirculations were expected [Klymak and Gregg, 1998] and observed in the across-fjord transect just to the north of the pass (data not shown). An implication of the flow intensification within the pass was that the ADCP backscatter signal became widespread throughout the water column in the region over the

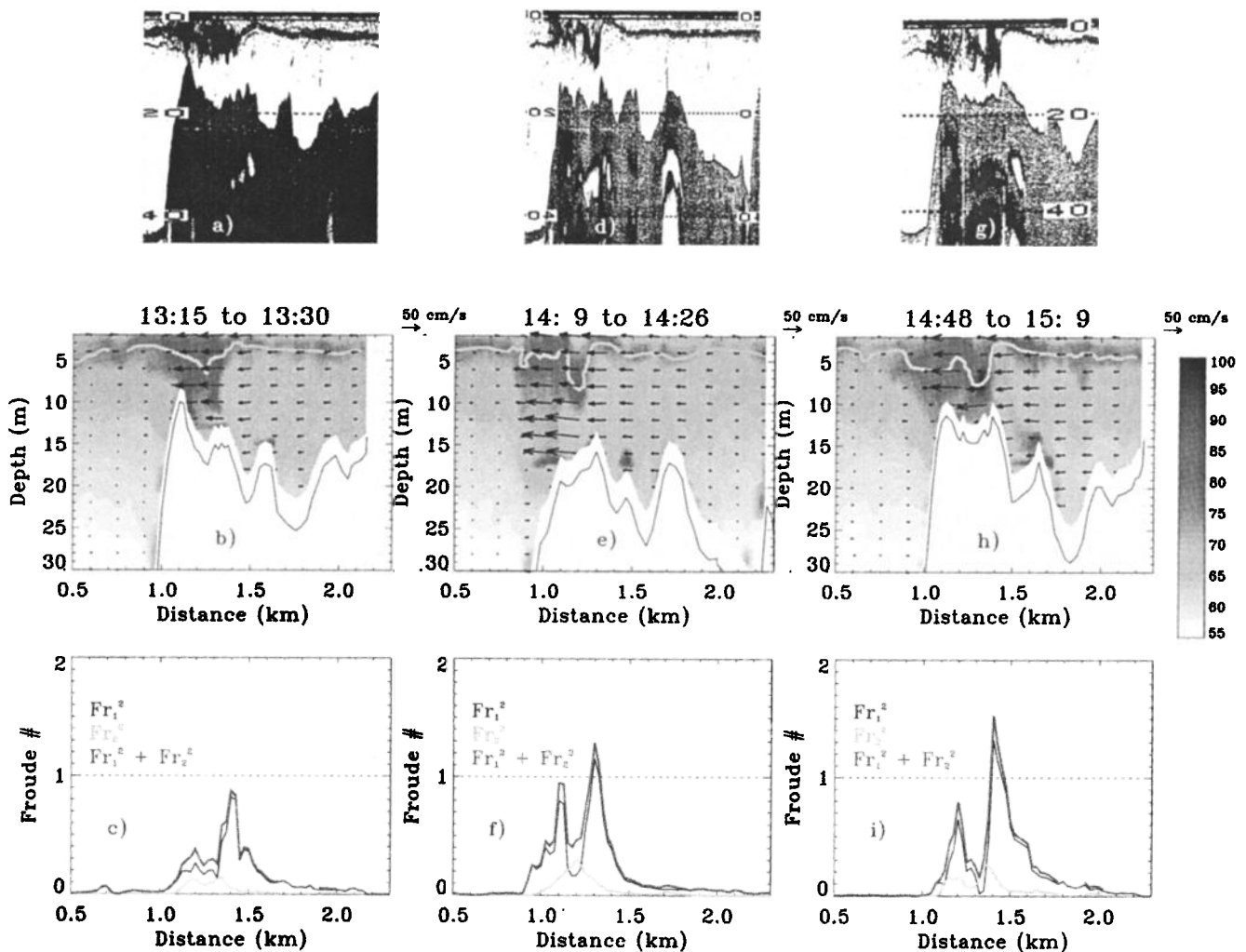


Figure 4. Along-fjord sections of (a, d, g) echo sounder backscatter, (b, e, h) ADCP flow and backscatter fields, and (c, f, i) layer and composite Froude numbers during flood flow. North (toward the head of the fjord) is to the left, and south (toward the mouth of the fjord) is to the right. The echo sounder traces of Figures 4a, 4d, and 4g are approximately aligned with the middle and lower panels. The times shown on Figures 4b, 4e, and 4h are GMT on January 12, 1998. Here flow is represented by vectors and ADCP backscatter by shaded contours at intervals of 5 decibels. Flow and backscatter scales are given to the right. Maximum backscatter positions along the pass are denoted by the thick, gray line that resembles the echo sounder trace. Flow vectors are shown every 2 m in the vertical and every 150 m in the horizontal. The bottom profile is shown as the black continuous line. The area of hampered quality in the velocity data (owing to ADCP side lobe effects) is masked in white just above the bottom profile.

sill (Figure 4b). This represented increased instabilities and vertical mixing at that location [e.g., *Farmer and Armi, 1999*].

The changes of the pycnocline depth along the pass were consistent with the distributions of the composite Froude number, G^2 (Figure 4c), where

$$G^2 = F_1^2 + F_2^2, \quad (1)$$

and F_1^2 and F_2^2 are the Froude numbers of the upper and lower layer, respectively. Also, $F_1^2 = u_1^2/(g'h_1)$ and $F_2^2 = u_2^2/(g'h_2)$, where h_1 and h_2 are the upper and lower layer thickness, u_1 and u_2 are the depth-averaged layer velocities, and g' is the reduced gravity (equal to $g \Delta \rho/\rho$, where g is the acceleration due to gravity and $\Delta \rho$ is the density contrast between the buoyant layer and the dense layer). The estimates of layer Froude numbers followed *Farmer and Armi* [1988] with $\Delta \rho$ of 8 kg/m^3 , as observed in Paso

Galvarino. The distribution of $G^2(x)$ illustrated the hydraulic state of the flow at each portion of the pass and showed that the flow was subcritical across the pass before maximum flood. As water flowed through the pass it accelerated at the constriction (between 1.3 and 1.4 km in Figure 4e). The flow decelerated rapidly to the north of the pass, which coincided with the pycnocline returning to the position it had upstream (relative to the tidal flow) of the pass.

Around maximum flood (Figures 4d through 4i), as the northward barotropic flow increased, the strength of the backscatter signal increased within the pass and an internal hydraulic jump became obvious. The internal motion activity was evidenced by well defined oscillations within the pass and by the pronounced upward bulging of the pycnocline, sometimes referred to as a rarefaction [e.g., *Baines, 1995*], just to the south (or upstream) of the constriction. These responses were observed both in the echo sounder images (Figures 4d and 4g) and in the maximum values of

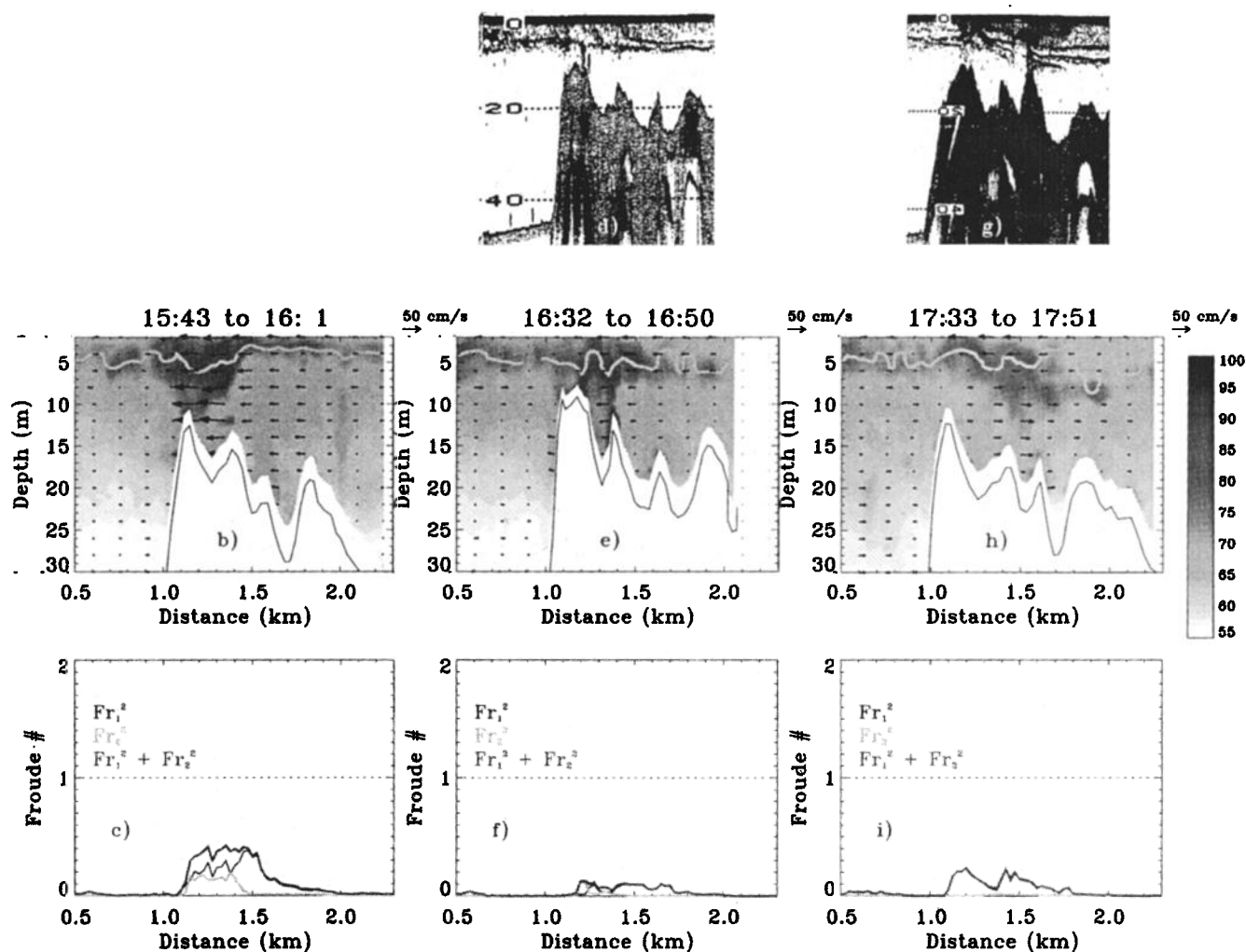


Figure 5. Same as Figure 4, but for late flood (echo sounder trace was not available for panel a).

the backscatter (Figures 4e and 4h). The enhanced backscatter signal appeared again toward the north end of the pass, i.e., leeward (relative to the direction of tidal forcing) of the point of a sharp pycnocline drop (~1.3–1.4 km). This was consistent with the expected increase in vertical mixing produced by stronger tidal flows. Also, transitions from subcritical to supercritical flow and back to subcritical developed within the pass during these flood stages (Figures 4f and 4i). The supercritical area within the pass became well defined during these periods of strongest flood currents. Sharp supercritical-to-subcritical transitions were reflected by the rapid upward excursion of the pycnocline leeward of the section constriction as expected from an internal hydraulic jump [Turner, 1973; Baines, 1995]. The jump seemed stationary as long as the magnitude of the barotropic flow remained comparable to c_s ($= [g'H]^{1/2}$, where H is the total water column depth).

Toward the end of flood and early ebb, the pycnocline did not seem affected by the morphology of the pass as it remained at approximately the same depth throughout the domain sampled (Figure 5). Early ebb corresponded to a two-layer flow with surface inflow (still flooding weakly) and bottom outflow (already ebbing) (Figure 5h). This pattern opposed the expected density-induced circulation (near-surface outflow and near-bottom inflow) and resulted

from the upward propagation of the phase of the tidal flow due to bottom friction, i.e., because of tidal phases occurring earlier near the bottom relative to the surface [e.g., Valle-Levinson and Lwiza, 1995; Valle-Levinson et al., 1998]. The ADCP backscatter signal intensified within (relative to outside of) the pass but not as markedly as around maximum flood. In addition, the flow remained subcritical during this tidal stage as G^2 remained lower than unity.

During the early ebb stages (Figure 6), the pycnocline dropped around the narrowest section and generated internal oscillations of relatively high wave number (Figures 6a, 6d, and 6g). The location where the internal oscillations were recorded by the echo sounder coincided with the area of intensified ADCP backscatter (Figures 6b, 6e, and 6h) and represented an area of instabilities and vertical mixing. The flow within the pass again became in the same direction throughout the water column. The ADCP backscatter now intensified to the south of the narrowest section, at a distance of 1.3–1.4 km. This was consistent with the observations during flood in the sense that the intensified backscatter signal appeared leeward, relative to the predominant tidal flow, of the narrowest section. The intense backscatter signal, which represented the region of enhanced instabilities and vertical mixing, extended further leeward (to the south in this case) than during flood. This resulted from the fact

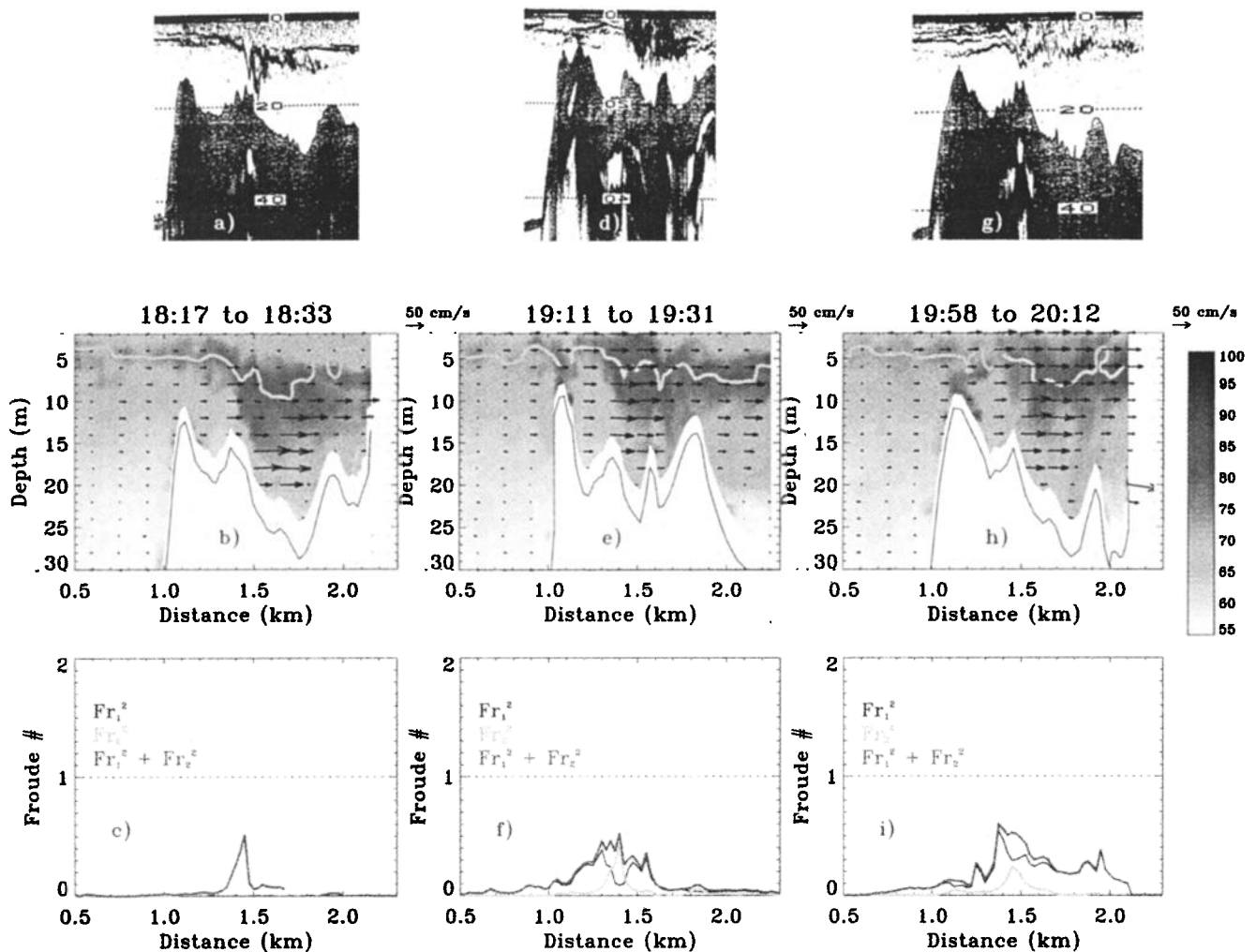


Figure 6. Same as Figure 4, but for early and maximum ebb.

that the distance between the point of pycnocline drop and the southern end of the pass was longer than the distance between the pycnocline drop and the northern end. At the leeward end of the pass, the flow decelerated because of widening of the coastline and deepening of the bathymetry and therefore vertical mixing must have decreased. The composite Froude number again showed subcritical conditions over the entire domain, although critical conditions approached at the narrowest section as ebb flow intensified (Figures 6c, 6f, and 6i).

At around maximum ebb, the pycnocline bulged up just upstream of the narrowest section (Figures 7a, 7b, 7d, and 7e), similarly to the pycnocline bulging that occurred around maximum flood (Figures 4d and 4g). Also, internal hydraulic jumps developed leeward of the pycnocline drop at the narrowest section and were likely caused by the relatively short transitions from supercritical to subcritical flows (Figure 7c). This looks like a case of maximal control as two critical points appeared within the pass at a distance of ~ 200 m. In contrast to flood, the slope of the pycnocline changed sign at the transition from subcritical to supercritical flow. Toward the end of ebb, the upward propagation of the tidal phase (flood occurring first at the bottom and then at the surface) resulted in near-surface outflow combined with near-bottom inflow (Figure 8b). This was in contrast to the

two-layer flows that appeared at the end of flood and suggested an irrelevant influence of the horizontal density gradient in shaping the flows. Otherwise, the exchange flows should have been consistent at both periods of slack waters. Nonetheless, the pycnocline position and the G^2 distribution were very similar between end of ebb and end of flood periods. The pycnocline did not seem to be affected by the morphology of the pass and the flow was subcritical everywhere (Figure 8c). Continuing over the tidal cycle, the early flood stages reflected similar conditions of pycnocline oscillations as the early ebb phases. The pycnocline oscillated with relatively high wave numbers leeward of the narrowest section (Figures 8d, 8e, 8g, and 8h), but the flow seemed to remain subcritical everywhere (Figures 8f and 8i).

5. Assessment of Observations in the Context of Theory

The morphology of the pass and the density of its waters characterize Paso Galvarino as a dynamically short pass, according to Helfrich [1995]. The dynamic length of a pass γ can be determined from the ratio of the length of the internal motion λ_i to the length of the pass L , i.e., $\gamma = \lambda_i/L$. Physically, this ratio represents the along-fjord distance (λ).

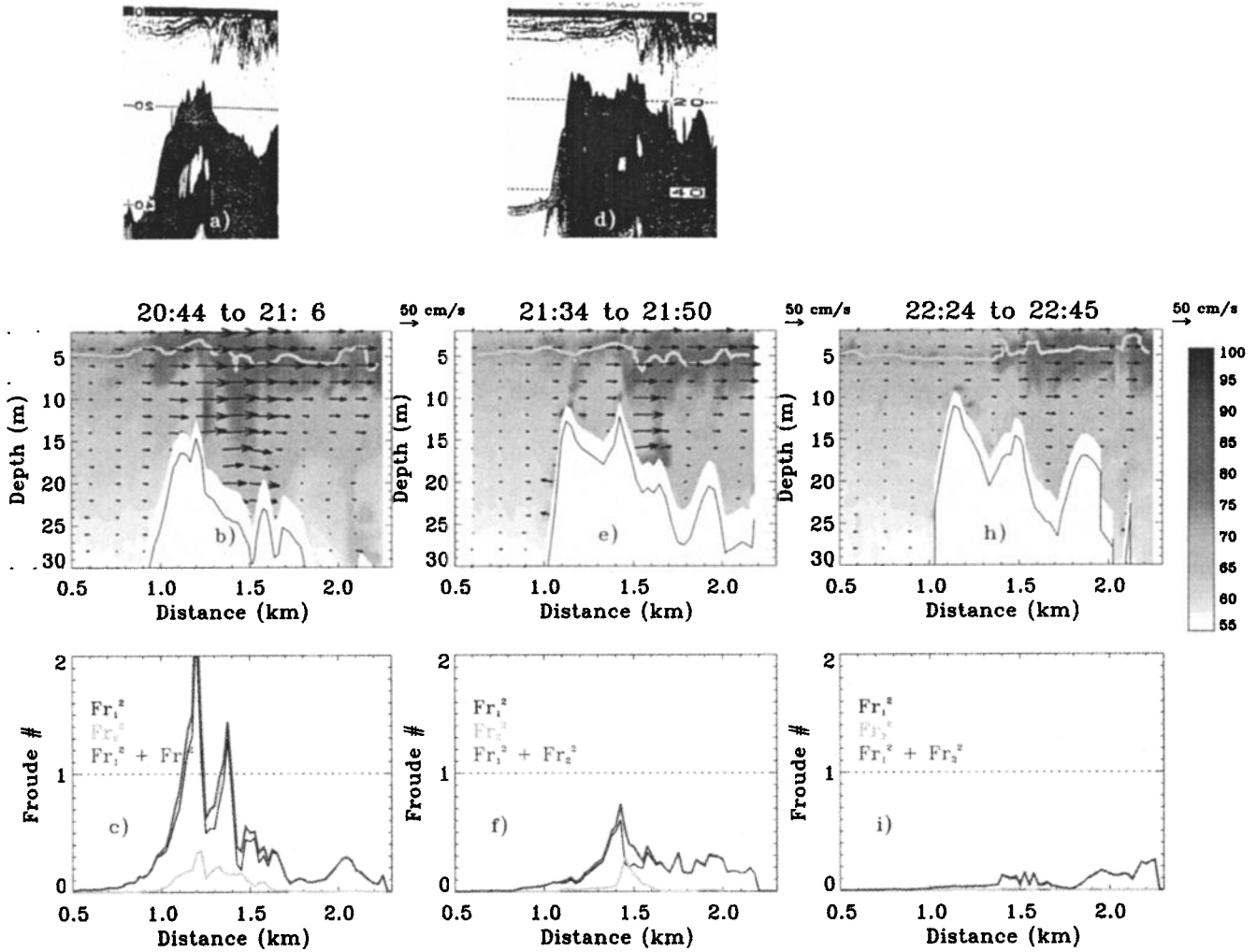


Figure 7. Same as Figure 4, but for maximum and late ebb (echo sounder trace was not available for panel g).

that a particle would be carried by the density-induced motion during one forcing period T , relative to L . The length λ , equals the phase speed of the internal gravity wave c_g multiplied by T , or,

$$\gamma = \frac{c_g T}{L} = \frac{\sqrt{g' H T}}{L}, \quad (2)$$

where g' and H are defined as before. For Paso Galvarino, L is 1.5 km and T is 12.42 hours. These properties yield $\gamma > 10$, i.e., a dynamically short pass. In a short pass, the dynamics are governed by quasi-steady hydraulics [Farmer and Denton, 1985; Farmer and Armi, 1986]. This means that the local accelerations are negligible relative to the advective accelerations. This was true in Paso Galvarino between the ~2 hours that preceded and the ~2 hours that followed maximum currents. During those periods, totaling 8 of the 12 hours sampled, the local accelerations were typically of the order of 10^{-5} m/s^2 . In contrast, the advective accelerations at the ends of the pass, where convergences/divergences were strongest (0.2 m/s in 100 m), were around 10^{-3} to 10^{-4} m/s^2 .

The theory for steady, uniform (upper and lower layer flowing in the same direction), two-layer flow over an obstacle or contraction and even the theory for a single-layer flow over an obstacle may be used to interpret several

aspects of the observations at Paso Galvarino. In particular, the change of sign of the pycnocline slope at the narrowest section related to the direction of barotropic flow as well as the occurrence of hydraulic jumps and rarefactions may be explained following the theory presented by Baines [1995]. In that theory, the hydraulic state of flow over an obstacle may be described from three dimensionless numbers: (1) the ratio of the unperturbed (far away from the obstacle) lower layer thickness h_{20} to the total water column depth ($r = h_{20}/H$), (2) the ratio of the maximum sill height h_m to the unperturbed lower layer thickness ($H_m = h_m/h_{20}$), and (3) the Froude number of the unperturbed flow F_u^2 , which is the undisturbed flow speed U divided by the internal gravity wave speed ($F_u^2 = U^2/[r(1-r)c_g^2]$). As Baines [1995] suggests, the depiction based on these three numbers is relevant to motion resulting from towing an obstacle through a resting fluid, or suddenly placing an obstacle in the path of a moving fluid, or to motion initiated by an externally imposed pressure gradient. These conditions are consistent with the onset of ebb or flood tide.

The two-layer flow properties may be extracted from expressions of conservation of mass and the Bernoulli equation in terms of H_m versus F_u curves for different values of r [see Baines, 1995]. Similarly, for single-layer theory, the flow properties may be represented on a H_m versus F_u

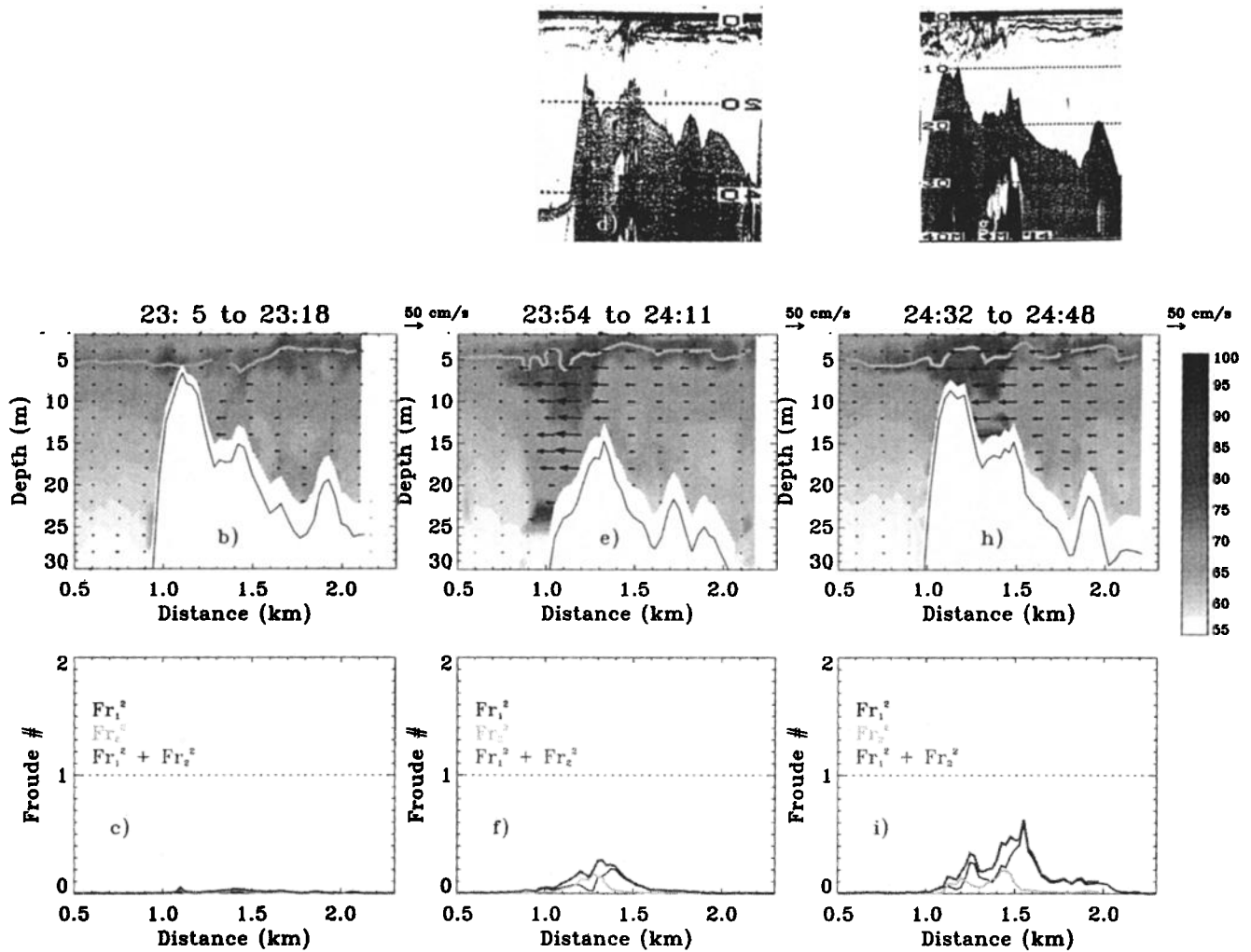


Figure 8. Same as Figure 4, but for early flood (echo sounder trace was not available for panel a).

diagram (Figures 9a and 9b) where the observations at the narrowest section of Paso Galvarino have been portrayed for different phases of the tidal cycle. The values of F_u at the narrowest section remained below 0.1, and those of H_m were around 0.9. Single-layer theory then predicts these observations to alternate between subcritical conditions and “partially blocked flow with lee jump (downstream hydraulic jump)” (Figure 9b). Furthermore, for the range of values of F_u and H_m observed, this theory predicts that a hydraulic jump should be stationary on the leeward side of the sill [Baines, 1995] as around maximum flood and ebb (Figures 4d, 4g, and 7a).

The same hydraulic depiction may be drawn from two-layer theory for which a value of r needs to be defined. In this application at Paso Galvarino $r \approx 0.88$ (35 m/40 m), which slightly modifies the curve on the F_u - H_m plane that separates subcritical flow from partially blocked flow with downstream jump, i.e., the dash-dot curve in Figure 9b denotes the transition from subcritical to supercritical flow. Critical flow conditions should then appear at certain values of F_u observed, which are essentially the same as those predicted by one-layer theory. Also, this theory predicts that no hydraulic jumps form upstream of the sill but does anticipate the development of rarefactions as manifested by the observed bulging of the pycnocline before the sharp drop

at the narrowest section (Figures 4 and 7). Although the sharp drops of the pycnocline at Paso Galvarino tend to occur at the narrowest section, not at the shallowest point of the sill, the two-layer theory for uniform flow over an obstacle yields explanations that are consistent with observations.

In turn, the theory of two-layer flow through a constriction [e.g., *Armi, 1986; Baines, 1984*] predicts similar behavior as that depicted above plus the possible development of a “virtual control” section where the flow is critical upstream of the constriction. The consistency of the explanations offered by theory of single and two-layer uniform flow over an obstacle with those of two-layer flow through a contraction may be explored on a Froude number plane derived from continuity and Bernoulli equations and that has the form [e.g. *Baines, 1995*]:

$$r = \frac{F_2^{-2/3} (1 + 0.5F_2^2) - 0.5q_f^{2/3} F_1^{4/3}}{F_2^{-2/3} + q_f^{2/3} F_1^{-2/3}}, \quad (3)$$

where q_f is the ratio of the transport in the upper layer q_1 (in cubic meters per second) relative to the lower layer q_2 . A virtual control is identified on the Froude number plane if $r < 1/[1+q_f]$. The layer Froude numbers observed in and

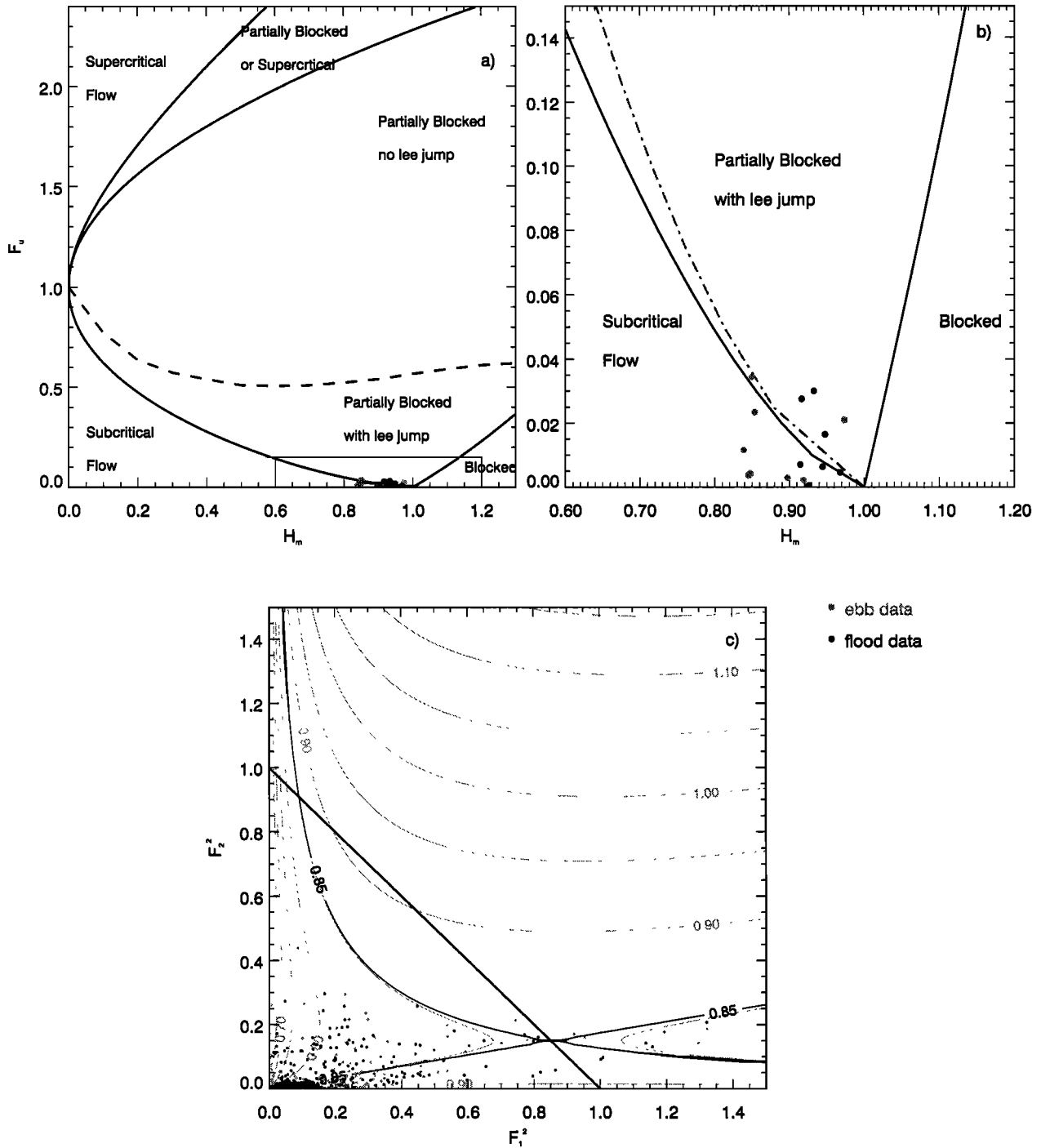


Figure 9. (a) Solutions of single-layer uniform flow past an obstacle in the H_m versus F_u plane with the different types of flows expected (adapted from Baines [1995]). The observations at the narrowest section of Paso Galvarino are represented by small, filled circles for flood and ebb flows. (b) Same as Figure 9a, but showing an enlargement of the portion of the diagram germane to our observations and the solution of two-layer uniform flow that separates subcritical from critical flow (dash dot line). (c) Solutions of the two-layer uniform flow through a constriction in the F_1^2 versus F_2^2 plane for $q_f = 0.175$ (adapted from Armi [1986]; and Baines [1995]) with our observations represented by dots for flood and ebb flows throughout the domain. The light contours represent different values of r according to (3). The darkest contour represents $r = 1/(1+q_f)$, and the straight line is where $G^2 = 1$. All the observations of undisturbed flow correspond to $F_1^2 < 0.1$ and $F_2^2 < 0.05$ thus falling above $r = 0.85$. A thorough discussion of the representation in Figure 9c is given by Baines [1995, 3.10.1].

around Paso Galvarino showed a few transitions from subcritical to supercritical flow (Figure 9c) but no development of “virtual control” as all of the observations start at $r > 1/[1 + q_f]$. Using q_f of 0.175 (unidirectional flow with the bulk of the unperturbed transport in the lower layer) yields

$r > 0.85$ at the location of unperturbed flow, as observed. The results portrayed on Figure 9 thus exhibit consistencies among single and two-layer unidirectional flow over an obstacle and two-layer unidirectional flow through a constriction. These theories predict the behavior of the flow and the

pycnocline as seen in Paso Galvarino if the unidirectional flow is prescribed initially at either side of the morphologic constriction according to the direction of the tidal forcing, which would determine the sign of the slope of the pycnocline drop.

The change of sign of the pycnocline drop at the narrowest section has also been described in numerical experiments. For example, *Hibiya et al.* [1998] considered the influence of barotropic forcing on flows over a sill with an initially stable two-layer water column with zero horizontal density gradient. Their numerical solutions showed a drop of the pycnocline on the leeward side of the sill relative to the tidal flow. Although *Hibiya et al.* did not discuss it, the sign of the pycnocline slope at the control point changed from flood to ebb and the steepness of the pycnocline drop was proportional to the strength of tidal forcing. Those numerical results and the observations presented here were also consistent in the tidally averaged properties.

The observed tidally averaged flow and backscatter fields indicated intensified vertical mixing within the pass (Figure

10a). Increased mixing, shown by increased backscatter in Figure 10a, should have caused upper layer densities in the pass to be higher than the upper layer densities outside the pass. Similarly, the mean lower layer densities inside the pass should have been lower than the lower layer densities outside. These density distributions are suggested by the distribution of the mean backscatter field in and at either side of the pass. The resulting mean density field caused an apparent three-layer flow consisting of near-surface flow from either side of the pass directed toward the pass, mean flow directed away from the pass at middepth, and near-bottom flow toward the pass. North of the sill (distances < 0.9 km in Figure 10a) the three-layer mean flow was not apparent, and a region of convergent flow centered at a depth of ~11 m. This flow convergence suggested the development of secondary flows associated with the rapid change in bathymetry and coastline. The three-layer pattern that seems to emerge from the observations is presented schematically in Figure 10b. The near-surface and near-bottom flow converging toward the sill and the midlayer diverging away

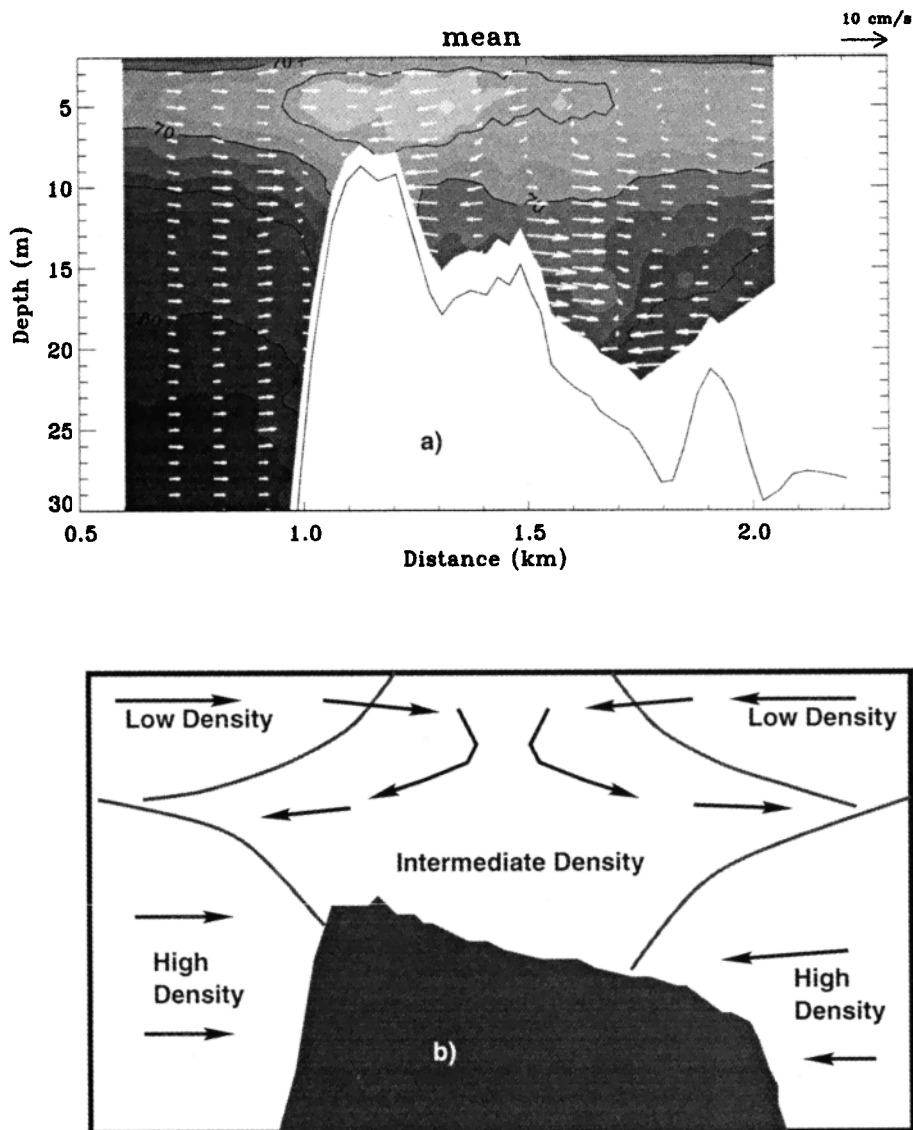


Figure 10. (a) Tidally averaged flow (vectors) and backscatter fields (shaded contours) at Paso Galvarino. (b) Schematic representation of the mean flow and density fields in a pass where vertical mixing is enhanced, as derived from the numerical experiments of *Hibiya et al.* [1998] and the observations shown in Figure 10a.

from the sill were in agreement with the results of *Hibiya et al.* [1998] in their numerical simulations of enhanced mixing over a sill. In those numerical results, the three-layer pattern was better developed during spring tides, when mixing intensified the horizontal density gradients. The suggestive three-layer pattern observed could be one of the few examples where it has been documented with field observations. The increased mixing within the pass should enhance the redistribution of dissolved and suspended materials and bolster the productivity within this region. In fact, various fishes and mammals were observed during this study roaming within the pass.

6. Summary

Underway velocity profiles obtained with an acoustic Doppler current profiler (ADCP) were combined with acoustic backscatter measurements from an echo sounder and from the ADCP itself in order to better understand the intratidal variability of flows through a sill-contraction combination in a Chilean pass, Paso Galvarino. The vertical gradient of the ADCP backscatter and the echo sounder trace were used to describe the changes in the pycnocline depth along the pass and with time. The flow and pycnocline distributions showed similarities from flood to ebb periods. Within the pass, the flow was practically in the same direction throughout the water column except around slack periods. A transition from subcritical to supercritical flow was identified during the periods of maximum unidirectional flow at the narrowest section of the pass (Figure 1). At this transition the pycnocline dropped abruptly, and the slope of this drop changed sign with the reversal of the barotropic flow. Around maximum tidal flows (flood or ebb), the pycnocline bulged upward just upstream of the transition as the tidal forcing initiated a rarefaction, i.e., an internal oscillation. Also around maximum flows, an internal hydraulic jump developed on the leeward side of the transition section and internal oscillations of high wave number were superimposed on the larger bulges and jumps. The ADCP recorded these oscillations as intensified backscatter downstream of the pycnocline drop, thus suggesting increased mixing over those areas. The area of intensified backscatter signal was greater during ebb than during flood periods because of the longer distance from the control point to the end of the pass, where the current converged rapidly. The magnitude and extent of the internal oscillations suggested that they are important to the biota of the system as they can redistribute dissolved and suspended materials to and from the bottom of the pass with every tidal cycle. In fact, the tidally averaged fields indicated increased vertical mixing within the pass and the development of a three-layer flow that was consistent with the density field generated by vertical mixing.

Acknowledgments. This study was funded by the Chilean National Environmental Commission. The captain and crew of the R/V *Arturo Pratt* are gratefully acknowledged for their commitment. R.C. Kidd provided invaluable help in the field, and A. Figueroa assisted in the data collection. The comments of L. Atkinson on the manuscript are greatly appreciated. Early conversations with E. D'Asaro, F. Henyey, and J. Klymak are gratefully acknowledged. Two anonymous reviewers made very valuable suggestions that substantially improved the original version of this manuscript.

References

- Armi, L., The hydraulics of two flowing layers with different densities, *J. Fluid Mech.*, 163, 27-58, 1986.
- Armi, L., and D.M. Farmer, Maximal two-layer exchange through a contraction with barotropic net flow, *J. Fluid Mech.*, 164, 27-51, 1986.
- Baines, P.G., A unified description of two-layer flow over topography, *J. Fluid Mech.*, 146, 127-167, 1984.
- Baines, P.G., *Topographic Effects in Stratified Flows*, 482 pp., Cambridge Univ. Press, New York, 1995.
- Borenäs, K.M., and L.J. Pratt, A review of rotating hydraulics, in *The Physical Oceanography of Sea Straits*, edited by L.J. Pratt, pp. 321-341, Kluwer Acad., Norwell, Mass., 1990.
- Bormans, M., and C. Garrett, The effects of rotation on the surface inflow through the strait of Gibraltar, *J. Phys. Oceanogr.*, 19, 1535-1542, 1989.
- Bryden, H.L., and T.H. Kinder, Recent progress in strait dynamics, *U.S. Natl. Rep. Int. Union Geod. Geophys. 1987-1990, Rev. Geophys.*, 29, 617-631, 1991.
- Cudaback, C.N., and D.A. Jay, Formation of the Columbia River Plume: Hydraulic control in action? in *Buoyancy Effects on Coastal and Estuarine Dynamics, Coastal and Estuarine Stud.* vol. 53, edited by David G. Aubrey and Carl T. Friedrichs, pp. 139-154, AGU, Washington, D.C., 1996.
- Dalziel, S.B., Rotating two-layer sill flows, in *The Physical Oceanography of Sea Straits*, edited by L.J. Pratt, pp. 343-371, Kluwer Acad., Norwell, Mass., 1990.
- Farmer, D.M., and L. Armi, Maximal two-layer exchange over a sill and through the combination of a sill and contraction with barotropic flow, *J. Fluid Mech.*, 164, 53-76, 1986.
- Farmer, D.M., and L. Armi, The flow of Atlantic water through the Strait of Gibraltar, *Prog. Oceanogr.*, 21, 1-105, 1988.
- Farmer, D.M., and L. Armi, The generation and trapping of solitary waves over topography, *Science*, 283, 188-190, 1999.
- Farmer, D.M., and R.A. Denton, Hydraulic control flow over the sill in Observatory Inlet, *J. Geophys. Res.*, 90(C5), 9051-9068, 1985.
- Farmer, D.M., and H.J. Freeland, The physical oceanography of fjords, *Prog. Oceanogr.*, 12, 147-220, 1983.
- Farmer, D.M., and J.D. Smith, Tidal interaction of stratified flow with a sill in Knight Inlet, *Deep Sea Res., Part A*, 27, 239-254, 1980.
- Gan, J., and R.G. Ingram, Internal hydraulics, solitons and associated mixing in a stratified sound, *J. Geophys. Res.*, 97(C6), 9669-9688, 1992.
- Geyer, R.W., Time-dependent, two layer flow over a sill, in *The Physical Oceanography of Sea Straits*, edited by L.J. Pratt, pp. 421-432, Kluwer Acad., Norwell, Mass., 1990.
- Geyer, R.W., and G.A. Cannon, Sill processes related to deep water renewal in a fjord, *J. Geophys. Res.*, 87(C10), 7985-7996, 1982.
- Gill, A.E. The hydraulics of rotating-channel flow, *J. Fluid Mech.*, 80, 641-671, 1977.
- Gill, A.E., *Atmosphere-Ocean Dynamics*, 662 pp., Academic, San Diego, Calif., 1982.
- Griffin, D.A., and P.H. Le Blond, Estuary/ocean exchange controlled by spring-neap tidal mixing, *Estuarine Coastal Shelf Sci.*, 30, 275-305, 1990.
- Hauray, L.R., M.G. Briscoe, and M.H. Orr, Tidally generated internal wave packets in Massachusetts Bay, U.S.A.: Preliminary physical and biological results, *Nature*, 278, 312-317, 1979.
- Hellfrich, K.R., Time-dependent two-layer hydraulic exchange flows, *J. Phys. Oceanogr.*, 25, 359-373, 1995.
- Hibiya, T., and P.H. LeBlond, The control of fjord circulation by fortnightly modulation of tidal mixing processes, *J. Phys. Oceanogr.*, 23, 2042-2052, 1993.
- Hibiya, T., M. Ogasawara, Y. Niwa, A numerical study of the fortnightly modulation of basin-ocean water exchange across a tidal mixing zone, *J. Phys. Oceanogr.*, 28, 1224-1235, 1998.
- Johnson, G.C., and D.R. Ohlsen, Frictionally modified rotating hydraulic channel exchange and ocean outflows, *J. Phys. Oceanogr.*, 24, 66-77, 1994.
- Killworth, P.D., Flow properties in rotating, stratified hydraulics, *J. Phys. Oceanogr.*, 22, 997-1017, 1992.
- Killworth, P.D., and N.R. McDonald, Maximal reduced-gravity flux in rotating, stratified hydraulics, *Geophys. Astrophys. Fluid Dyn.*, 70, 31-40, 1993.
- Klymak, J.M., and M.C. Gregg, Three-dimensional circulation in

- Knight Inlet, *Eos Trans. AGU*, 79(1), Ocean Sci. Meet. Suppl., 104, 1998.
- Marsden, R.F., and K.C. Greenwood, Internal tides observed by an acoustic Doppler current profiler, *J. Phys. Oceanogr.*, 24, 1097-1109, 1994.
- Matsuura, T., and T. Hibiya, An experimental and numerical study of the internal wave generation by tide-topography interaction, *J. Phys. Oceanogr.*, 20, 506-521, 1990.
- McClimans, T.A., Role of laboratory experiments and models in the study of sea strait processes, in *The Physical Oceanography of Sea Straits*, edited by L.J. Pratt, pp. 373-388, Kluwer Acad., Norwell, Mass., 1990.
- Pickard, G.L., Some physical oceanographic features of inlets of Chile, *J. Fish. Res. Bd. Can.*, 28, 1077-1106, 1971.
- Pratt, L. J., and P.A. Lundberg, Hydraulics of rotating strait and sill flow, *Annu. Rev. Fluid Mech.*, 23, 81-106, 1991.
- Pratt, L. J., W. Johns, S.P. Murray, and K. Katsumata, Hydraulic interpretation of direct velocity measurements in the Bab al Mandab, *J. Phys. Oceanogr.*, 29, 2769-2784, 1999.
- Silva, N., H.A. Sievers, and R. Prado, Características oceanográficas y una proposición de circulación para algunos canales australes de Chile entre 41° 20'S and 46° 40'S, *Rev. Biol. Mar., Valparaíso*, 30(2), 207-254, 1995.
- Stacey, M.W., The interaction of tides with the sill of a tidally energetic inlet, *J. Phys. Oceanogr.*, 14, 1105-1117, 1984.
- Stigebrandt, A., On the effect of barotropic current fluctuations on the two-layer transport capacity of a constriction, *J. Phys. Oceanogr.*, 7, 118-122, 1977.
- Stommel, H., and H.G. Farmer, Abrupt change in width in two layer open channel flow, *J. Mar. Res.*, 11, 205-214, 1952.
- Stommel, H., and H.G. Farmer, Control of salinity in an estuary by a transition, *J. Mar. Res.*, 12, 13-20, 1953.
- Trump, C.L., and G. Marmorino, Calibrating a gyrocompass using ADCP and DGPS data, *J. Atmos. Oceanic Technol.*, 14(1), 211-214, 1997.
- Turner, J.S., *Buoyancy Effects in Fluids*, 367 pp., Cambridge Univ. Press, New York, 1973.
- Valle-Levinson, A., and K.M.M. Lwiza, Effects of channels and shoals on the exchange between the lower Chesapeake Bay and the adjacent ocean, *J. Geophys. Res.*, 100(C9), 18,551-18,563, 1995.
- Valle-Levinson, A., and R.E. Wilson, Effects of sill bathymetry, oscillating barotropic forcing and vertical mixing on estuary/ocean exchange, *J. Geophys. Res.* 99(C3), 5149-5169, 1994a.
- Valle-Levinson, A., and R.E. Wilson, Effects of sill processes and barotropic forcing on exchange in Eastern Long Island Sound, *J. Geophys. Res.*, 99(C6), 12,667-12,681, 1994b.
- Valle-Levinson, A., C. Li, T.C. Royer, and L.P. Atkinson, Flow patterns at the Chesapeake Bay entrance, *Cont. Shelf Res.*, 18(10), 1157-1177, 1998.

F. Jara, Laboratorio de Ecología Acuática, Casilla 1060, Puerto Montt, Chile.

C. Molinet, Centro Universitario de La Trepananda, Universidad Austral de Chile, Coyhaique, Chile.

D. Soto, Facultad de Pesquerías y Oceanografía, Universidad Austral de Chile, Puerto Montt, Chile.

A. Valle-Levinson, Center for Coastal Physical Oceanography, Department of Ocean, Earth, and Atmospheric Sciences, Old Dominion University, Norfolk, VA 23529. (armoldo@ccpo.odu.edu)

(Received May 17, 1999; revised September 18, 2000; accepted October 19, 2000.)